AIAA JOURNAL
Vol. 42, No. 2, February 2004

Calculation of Transonic Internal Flows Using an Efficient High-Resolution Upwind Scheme

Ge-Cheng Zha* and Zongjun Hu†
University of Miami, Coral Gables, Florida 33124

A new efficient upwind scheme based on the concept of convective upwind and split pressure is developed. The upwinding of the convective term and the pressure split are consistent with their characteristic directions. The scheme has low diffusion to resolve accurately wall boundary layers and is able to capture crisp shock waves and exact contact discontinuities. The accuracy of the scheme is compared with other popularly used schemes including the Roe scheme, the Liou's latest advection upstream splitting method scheme (AUSM$^+$), the Van Leer scheme, and the Van Leer–Hänel scheme. The new scheme is tested for the one-dimensional Sod shock tube problem, one-dimensional slowly moving contact surface, supersonic flat plate laminar boundary layer, a transonic nozzle with oblique shock waves and reflections that do not align with the mesh lines, and a transonic inlet diffuser with shock wave/turbulent boundary-layer interaction. The test cases show that the new scheme is accurate, robust, and efficient.

Nomenclature

a	=	speed of sound
$\boldsymbol{D}$	=	numerical dissipation vector
$\boldsymbol{E}$	=	inviscid flux of quasi-one-dimensional Euler equations
$\boldsymbol{E}', \boldsymbol{F}', \boldsymbol{G}'$	=	inviscid flux vectors in ξ, η, and ζ directions
e	=	total energy per unit mass
$\boldsymbol{F}$	=	inviscid flux of quasi-one-dimensional Euler equations per unit area
$\boldsymbol{H}$	=	source term of quasi-one-dimensional Euler equations, total enthalpy
J	=	transformation Jacobian
$\boldsymbol{l}$	=	control volume interface area vectors, $l_x\boldsymbol{i} + l_y\boldsymbol{j} + l_z\boldsymbol{k}$
M	=	Mach number
p	=	static pressure
$\boldsymbol{Q}$	=	conservative variable vector
$\boldsymbol{R}', \boldsymbol{S}', \boldsymbol{T}'$	=	viscous flux vectors in ξ, η, and ζ directions
S	=	cross-sectional area of one-dimensional duct
T	=	right eigenvector matrix of the Jacobian matrix
U	=	normal contravariant velocity in ξ direction
$\boldsymbol{U}$	=	conservative variable vector of quasi-one-dimensional Euler equations multiplied by duct area
u, v, w	=	velocity in x, y, and z directions
$\boldsymbol{V}$	=	velocity vector, $u\boldsymbol{i} + v\boldsymbol{j} + w\boldsymbol{k}$
x, y, z	=	spatial coordinates in the Cartesian coordinate system
γ	=	specific heat ratio
Λ	=	eigenvalue matrix of the Jacobian matrix
ξ, η, ζ	=	spatial coordinates in the generalized coordinate system
ρ	=	density

Subscripts

i	=	cell index
L	=	left value
R	=	right value
t	=	time
$\frac{1}{2}$	=	control interface position

Superscripts

c	=	convective
$n, n+1$	=	time level index
p	=	pressure
$+$	=	upwind direction
$-$	=	downwind direction
$\sim$	=	Roe's average
$'$	=	flux vectors of H convective upwind and split pressure schemes, flux vectors in three-dimensional generalized coordinates

Received 13 June 2003; revision received 20 September 2003; accepted for publication 23 September 2003.

*Associate Professor, Department of Mechanical Engineering; zha@apollo.eng.miami.edu. Member AIAA.

†Ph.D. Student, Department of Mechanical Engineering.

I. Introduction

DEVELOPMENT of an accurate and efficient numerical scheme for compressible flow governing equations is essential due to the increasing engineering demand for aircraft and spacecraft design.[1] Such a scheme is particularly important when aircraft engine turbomachinery aeroelasticity problems are simulated using a fully coupled fluid/structural model, which is usually very CPU intensive. Hence, an accurate, efficient, and robust upwind scheme used as the Riemann solver to resolve shock waves, contact surface discontinuities, and wall boundary layers is very desirable.

To achieve efficiency and accuracy, efforts have been made to develop upwind schemes only using scalar dissipation instead of matrix dissipation, such as that of the Roe's flux difference splitting scheme.[2] The examples include advection upstream splitting method (AUSM) family of schemes represented by the latest scheme of AUSM$^+$,[3–7] the Van Leer–Hänel scheme (see Ref. 8), Edwards's low-diffusion flux splitting schemes (LDFSS),[9,10] Jameson's convective upwind and split pressure (CUSP) schemes and limiters[11–13] the schemes developed by Zha and Bilgen,[14] Zha,[15,16] etc.

Pioneered by Liou and Steffen,[3] and Liou,[5,6] the researchers seeking the scalar dissipation primarily follow the guideline that the velocity and pressure should be separated to consider their characteristics representing the physics of the convection and waves. These schemes were termed AUSM schemes, and Jameson provided the name CUSP schemes.[11–13] CUSP seems to reflect the physical meaning more precisely.

As pointed out by Jameson,[11–13] CUSP schemes can be basically categorized into two types, H-CUSP and E-CUSP. H-CUSP schemes have the total enthalpy from the energy equation in their convective vector, whereas E-CUSP schemes use the total energy

in the convective vector. Liou's AUSM family schemes, Van Leer–Hänel scheme (see Ref. 8), and Edwards's LDFSS[9,10] belong to the H-CUSP group. H-CUSP schemes may have the advantages to better conserve the total enthalpy for steady-state flows. The schemes developed by Zha and Bilgen[14] and Zha[15] belong to the E-CUSP group. Jameson suggested schemes for both groups.[11–13]

Even though the H-CUSP schemes such as AUSM family schemes have achieved great success, from the characteristic theory point of view, the schemes are not fully consistent with the disturbance propagation directions, which may affect the stability and robustness of the schemes. By splitting the eigenvalues of the Jacobians to convection (velocity) and waves (speed of sound), one will find that the convection terms only contain the total energy,[14] which will lead to the E-CUSP schemes. However, the early E-CUSP schemes could not handle contact discontinuities.[11–14] Borrowing from the AUSMDV scheme,[4] Zha used the interface speed of sound and made his E-CUSP scheme able to capture exact contact discontinuities. However, because of the lack of proper numerical dissipation, the scheme will generate odd–even pressure oscillations when applied to multidimensional flows.

The purpose of this paper is to develop a high-resolution E-CUSP scheme that is consistent with the characteristic directions and that is also accurate, efficient, and robust. The high resolution means that it can accurately resolve the wall boundary shear layers, shock wave, and contact discontinuities.

II. Numerical Scheme

A. Governing Equations

To describe the new scheme, we will begin with the quasi-one-dimensional Euler equations in Cartesian coordinates for inviscid flow:

$$\partial_t \boldsymbol{U} + \partial_x \boldsymbol{E} - \boldsymbol{H} = 0 \tag{1}$$

where

$$\boldsymbol{U} = S\boldsymbol{Q}, \qquad \boldsymbol{Q} = \begin{pmatrix} \rho \\ \rho u \\ \rho e \end{pmatrix}, \qquad \boldsymbol{E} = S\boldsymbol{F}$$

$$\boldsymbol{F} = \begin{bmatrix} \rho u \\ \rho u^2 + p \\ (\rho e + p)u \end{bmatrix}, \qquad \boldsymbol{H} = \frac{\mathrm{d}S}{\mathrm{d}x}\begin{pmatrix} 0 \\ p \\ 0 \end{pmatrix} \tag{2}$$

The following state equation is also employed:

$$p = (\gamma - 1)\left(\rho e - \tfrac{1}{2}\rho u^2\right) \tag{3}$$

where γ is the specific heat ratio with the value of 1.4 for ideal gas.

The finite volume method with the explicit Euler temporal integration is used to discretize the governing equations. It yields the following formulation at cell i:

$$\Delta \boldsymbol{Q}_i^{n+1} = \Delta t\left[-C\left(\boldsymbol{E}_{i+\frac{1}{2}} - \boldsymbol{E}_{i-\frac{1}{2}}\right) + \boldsymbol{H}_i / S_i\right]^n \tag{4}$$

where $C = 1/(\Delta x S_i)$. A numerical scheme is needed to evaluate the interface flux:

$$\boldsymbol{E}_{i+\frac{1}{2}} = S\boldsymbol{F}_{i+\frac{1}{2}} \tag{5}$$

B. Characteristics

To develop the scheme for $\boldsymbol{F}_{i+1/2}$, we need to analyze the characteristics first. It is well known that the eigenvalues of the Jacobian matrix are $u + a$, u, and $u - a$. That is,

$$\boldsymbol{A} = \frac{\partial \boldsymbol{F}}{\partial \boldsymbol{Q}} = \boldsymbol{T}\boldsymbol{\Lambda}\boldsymbol{T}^{-1} \tag{6}$$

where

$$\boldsymbol{T} = \begin{pmatrix} 1 & 1 & 1 \\ u - a & u & u + a \\ H - ua & \frac{1}{2}u^2 & H + ua \end{pmatrix}, \qquad \boldsymbol{\Lambda} = \begin{pmatrix} u - a & 0 & 0 \\ 0 & u & 0 \\ 0 & 0 & u + a \end{pmatrix}$$

Because of the homogeneous relationship between $\boldsymbol{Q}$ and $\boldsymbol{F}$, we have

$$\boldsymbol{F} = \boldsymbol{T}\boldsymbol{\Lambda}\boldsymbol{T}^{-1}\boldsymbol{Q} \tag{7}$$

The Steger–Warming scheme[17] and the Roe scheme[2] are directly based on the preceding characteristic relations. For supersonic flows, all of the eigenvalues are positive, and a numerical scheme can simply take the upwind differencing. The difficulty in constructing a Riemann solver for interface flux $\boldsymbol{F}$ appears in the subsonic regime, where the acoustic waves propagate in both the downstream and upstream directions. To separate the convective terms and wave terms, the eigenvalue matrix may be split as[14]

$$\boldsymbol{F} = \boldsymbol{T}\begin{pmatrix} u & 0 & 0 \\ 0 & u & 0 \\ 0 & 0 & u \end{pmatrix}\boldsymbol{T}^{-1}\boldsymbol{Q} + \boldsymbol{T}\begin{pmatrix} -a & 0 & 0 \\ 0 & 0 & 0 \\ 0 & 0 & a \end{pmatrix}\boldsymbol{T}^{-1}\boldsymbol{Q} = \boldsymbol{F}^c + \boldsymbol{F}^p \tag{8}$$

where

$$\boldsymbol{F}^c = u\begin{pmatrix} \rho \\ \rho u \\ \rho e \end{pmatrix}, \qquad \boldsymbol{F}^p = \begin{pmatrix} 0 \\ p \\ pu \end{pmatrix} \tag{9}$$

Obviously, the vector $\boldsymbol{F}^c$ has the eigenvalues of velocity and, hence, is the convective term. The vector $\boldsymbol{F}^p$ has the eigenvalues of speed of sound, which represent the acoustic waves propagating in each direction at subsonic regime. The preceding relations will lead to the E-CUSP schemes that have the total energy term in the convective vector $\boldsymbol{F}^c$.

Based on the separation of convective and wave terms in subsonic regime, Zha and Bilgen[14] and Zha[15,16] suggested treating the convective term $\boldsymbol{F}^c$ in a simple upwind manner and averaging the wave term $\boldsymbol{F}^p$ in both the upwind and downwind directions with the weight of $u \pm a$.

The H-CUSP schemes absorb the pressure term in the energy equation of $\boldsymbol{F}^p$ into the convective vector in terms of the total enthalpy. The convective vector and wave vector, hence, become

$$\boldsymbol{F}'^c = u\begin{pmatrix} \rho \\ \rho u \\ \rho H \end{pmatrix}, \qquad \boldsymbol{F}'^p = \begin{pmatrix} 0 \\ p \\ 0 \end{pmatrix} \tag{10}$$

where H is the total enthalpy

$$H = (\rho e + p)/\rho \tag{11}$$

The eigenvalues of $\boldsymbol{F}'^c$ are $(u, u, \gamma u)$, and the eigenvalues of $\boldsymbol{F}'^p$ are $[0, 0, -(\gamma - 1)u]$ (Ref. 12). These eigenvalues mean that the pressure vector $\boldsymbol{F}'^p$ only has downwind propagation, which does not reflect the true wave propagation, and, hence, the vector is not strictly the wave vector. Most of the H-CUSP schemes, such as the AUSM family schemes of Liou and Steffen,[3] Wada and Liou,[4] and Liou[5–7] average the pressure term $\boldsymbol{F}'^p$ in both the upwind and the downwind direction with the weight of $u \pm a$. Obviously, this is not consistent with the characteristics of $\boldsymbol{F}'^p$, which only has the downwind direction. Even though the upwinding treatment of the vector $\boldsymbol{F}'^c$ is justified according to its eigenvalues, the vector is not strictly the convective vector due to absorption of the pressure term in the energy equation.

C. New E-CUSP Scheme

A new E-CUSP scheme is developed that is consistent with the characteristic directions. Based on the characteristics of the vector $\boldsymbol{F}^c$ and $\boldsymbol{F}^p$, Zha and Bilgen suggested a simple flux vector splitting scheme at the subsonic regime[14] as follows:

$$\boldsymbol{F}_{\frac{1}{2}} = \frac{1}{2}\left[\boldsymbol{F}^c_L + \boldsymbol{F}^c_R\right] - \frac{1}{2}[(|u|\boldsymbol{Q})_R - (|u|\boldsymbol{Q})_L] + \frac{1}{2}\left\{\begin{bmatrix} 0 \\ p(1+M) \\ p(u+a) \end{bmatrix}_L + \begin{bmatrix} 0 \\ p(1-M) \\ p(u-a) \end{bmatrix}_R\right\} \tag{12}$$

For supersonic flow, it switches to a fully upwind scheme.

This scheme treats the convective vector $\boldsymbol{F}^c$ in an upwind manner and the pressure vector $\boldsymbol{F}^p$ with the eigenvalue $u \pm a$ weighted average from both the upwind and downwind directions. The pressure vector naturally transits to fully upwind in the supersonic regime. Most of the numerical dissipation terms of this scheme vanish with the velocity approaching zero. When the common interface speed of sound as suggested by Wada and Liou[4] is used, the scheme can handle exact contact discontinuities.[16] However, due to a lack of proper numerical dissipation, the scheme generates odd–even pressure oscillations when used for multidimensional flows.

To suppress the oscillations, the way to introduce the dissipation used by Wada and Liou for their AUSMD scheme[4] is borrowed to construct the convective term. First, the velocity u^+_L and u^-_R are introduced as

$$u^+_L = a_{\frac{1}{2}}\left\{(M_L + |M_L|)/2 + \alpha_L\left[\tfrac{1}{4}(M_L+1)^2 - (M_L + |M_L|)/2\right]\right\} \tag{13}$$

$$u^-_R = a_{\frac{1}{2}}\left\{(M_R - |M_R|)/2 + \alpha_R\left[-\tfrac{1}{4}(M_R-1)^2 - (M_R - |M_R|)/2\right]\right\} \tag{14}$$

where the interface speed of sound $a_{1/2}$, Mach number, and α are evaluated as

$$a_{\frac{1}{2}} = \tfrac{1}{2}(a_L + a_R) \tag{15}$$

$$M_L = \frac{u_L}{a_{\frac{1}{2}}}, \qquad M_R = \frac{u_R}{a_{\frac{1}{2}}} \tag{16}$$

$$\alpha_L = \frac{2(p/\rho)_L}{(p/\rho)_L + (p/\rho)_R}, \qquad \alpha_R = \frac{2(p/\rho)_R}{(p/\rho)_L + (p/\rho)_R} \tag{17}$$

An interface mass flux is introduced as

$$(\rho u)_{\frac{1}{2}} = \left(\rho_L u^+_L + \rho_R u^-_R\right) \tag{18}$$

Then the convective vector $\boldsymbol{F}^c$ is evaluated as

$$\boldsymbol{F}^c = \tfrac{1}{2}\left[(\rho u)_{\frac{1}{2}}\left(\boldsymbol{q}^c_L + \boldsymbol{q}^c_R\right) - |\rho u|_{\frac{1}{2}}\left(\boldsymbol{q}^c_R - \boldsymbol{q}^c_L\right)\right] \tag{19}$$

where

$$\boldsymbol{q}^c = \begin{pmatrix} 1 \\ u \\ e \end{pmatrix} \tag{20}$$

The pressure term in the momentum equation uses the pressure splitting formulations of AUSM$^+$,[5]

$$p_{\frac{1}{2}} = (\mathcal{P}^+ p)_L + (\mathcal{P}^- p)_R \tag{21}$$

where

$$\mathcal{P}^{\pm} = \tfrac{1}{4}(M \pm 1)^2(2 \mp M) \pm \alpha M(M^2-1)^2, \qquad \alpha = 3/16 \tag{22}$$

The pressure splitting in the energy equation uses the simple linear eigenvalues weighted average:

$$(pu)_{\frac{1}{2}} = \tfrac{1}{2}\left[p\left(u + a_{\frac{1}{2}}\right)\right]_L + \tfrac{1}{2}\left[p\left(u - a_{\frac{1}{2}}\right)\right]_R \tag{23}$$

The energy pressure term may also use the higher-order polynomial such as Van Leer's Mach number splitting[18]:

$$(pu)_{\frac{1}{2}} = \tfrac{1}{4}a_{\frac{1}{2}}[\,p(M+1)^2]_L - \tfrac{1}{4}a_{\frac{1}{2}}[\,p(M-1)^2]_R \tag{24}$$

However, the numerical experiments indicated that Eq. (24) is less robust and may generate oscillatory solutions. Hence, the linear pressure splitting of Eq. (23) is adopted. The drawback of the linear pressure splitting of Eq. (23) is that the first-order derivative is not continuous at the sonic point, similar to the Steger–Warming scheme.[17] This may cause some nonsmoothness at the sonic point when first-order scheme is used. When a scheme higher than first-order is used, the nonsmoothness disappears.[16]

In summary, the new E-CUSP scheme can be written as follows. For $|u| \le a$,

$$\boldsymbol{F}_{\frac{1}{2}} = \frac{1}{2}\left[(\rho u)_{\frac{1}{2}}\left(\boldsymbol{q}^c_L + \boldsymbol{q}^c_R\right) - |\rho u|_{\frac{1}{2}}\left(\boldsymbol{q}^c_R - \boldsymbol{q}^c_L\right)\right] + \begin{bmatrix} 0 \\ \mathcal{P}^+ p \\ \frac{1}{2}p\left(u + a_{\frac{1}{2}}\right) \end{bmatrix}_L + \begin{bmatrix} 0 \\ \mathcal{P}^- p \\ \frac{1}{2}p\left(u - a_{\frac{1}{2}}\right) \end{bmatrix}_R \tag{25}$$

For $u > a$,

$$\boldsymbol{F}_{\frac{1}{2}} = \boldsymbol{F}_L$$

For $u < -a$,

$$\boldsymbol{F}_{\frac{1}{2}} = \boldsymbol{F}_R$$

where the definitions of the different terms are given as Eq. (18) for $(\rho u)_{1/2}$, Eq. (20) for $\boldsymbol{q}^c$, Eq. (22) for $\mathcal{P}^{\pm}$, Eq. (15) for $a_{1/2}$, and Eq. (16) for Mach number. The definitions of the Mach number and the interface speed of sound are essential to capturing the exact contact discontinuities.

III. Numerical Dissipation

The low numerical dissipation at stagnation is important to resolve accurately wall boundary layers. Liou's AUSM$^+$ scheme has all of the numerical dissipation terms vanishing when the velocity approaches zero, which, hence, yields low numerical dissipation for wall boundary layers. For the new E-CUSP scheme, almost all of the numerical dissipation terms vanish with the velocity approaching zero, except one term in the energy equation due to the pressure splitting [Eq. (23)].

Assume $u = 0$: The numerical dissipation vector of the new E-CUSP scheme at stagnation is

$$\boldsymbol{D} = -\frac{a_{\frac{1}{2}}}{2}\begin{pmatrix} 0 \\ 0 \\ \delta p \end{pmatrix} \tag{26}$$

where

$$\delta p = p_R - p_L \tag{27}$$

The numerical dissipation of the Roe scheme at stagnation is

$$\boldsymbol{D}_{Roe} = -\frac{\tilde{a}_{\frac{1}{2}}}{2(\gamma-1)}\begin{pmatrix} (\gamma-1)\big/\tilde{a}^2_{\frac{1}{2}}\,\delta p \\ 0 \\ \delta p \end{pmatrix} \tag{28}$$

where the tilde indicates the Roe average.[2]

When Eqs. (26) and (28) are compared, it can be seen that the numerical dissipation of the new E-CUSP scheme for the continuity equation vanishes at $u=0$, whereas the Roe scheme has nonvanishing dissipation. For the energy equation, the two schemes have equivalent dissipation. For ideal gas with the $\gamma=1.4$, the coefficient of the Roe scheme energy dissipation term is 2.5 times larger than that of the new E-CUSP scheme.

In conclusion, even though there is one nonvanishing numerical dissipation term in the energy equation for the new E-CUSP scheme, the overall numerical dissipation of the new E-CUSP scheme is not greater than that of the Roe scheme. The Roe scheme is proved to be accurate to resolve wall boundary layers (see Ref. 19). Hence, it is expected that the new E-CUSP scheme should also have sufficiently low dissipation to resolve accurately wall boundary layers. This is indeed the case shown by the numerical experiment for a flat-plate boundary layer.

IV. Extension to Multidimensions

The three-dimensional Navier–Stokes equations in conservation law form and in generalized coordinates are given as

$$\frac{\partial \boldsymbol{Q}'}{\partial t}+\frac{\partial \boldsymbol{E}'}{\partial \xi}+\frac{\partial \boldsymbol{F}'}{\partial \eta}+\frac{\partial \boldsymbol{G}'}{\partial \zeta}=\frac{\partial \boldsymbol{R}'}{\partial \xi}+\frac{\partial \boldsymbol{S}'}{\partial \eta}+\frac{\partial \boldsymbol{T}'}{\partial \zeta} \tag{29}$$

where Q' is the conservative variable vector, and $\boldsymbol{R}'$, $\boldsymbol{S}'$, and $\boldsymbol{T}'$ are determined by the Reynolds average process to model the turbulence. To save the space, the contents of the viscous fluxes will not be given here; they may be found in standard computational fluid dynamics textbooks.

$\boldsymbol{Q}'$ and $\boldsymbol{E}'$ are given as

$$\boldsymbol{Q}'=\frac{1}{J}\begin{pmatrix}\rho\\ \rho u\\ \rho v\\ \rho w\\ \rho e\end{pmatrix},\qquad \boldsymbol{E}'=\begin{pmatrix}\rho U\\ \rho uU+l_x p\\ \rho vU+l_y p\\ \rho wU+l_z p\\ (\rho e+p)U\end{pmatrix} \tag{30}$$

where u, v, and w are the velocity components in the x, y, and z directions and U is the normal contravariant velocity in the ξ direction,

$$U=\boldsymbol{V}\cdot\boldsymbol{l}=ul_x+vl_y+wl_z \tag{31}$$

The vector $\boldsymbol{l}$ is the control volume interface area vector pointing in the direction normal to the interface with the magnitude equal to the interface area. Let $\Delta\xi=\Delta\eta=\Delta\zeta=1$, and then $\boldsymbol{l}$ is expressed as

$$\boldsymbol{l}=l_x\boldsymbol{i}+l_y\boldsymbol{j}+l_z\boldsymbol{k}=(1/J)(\xi_x\boldsymbol{i}+\xi_y\boldsymbol{j}+\xi_z\boldsymbol{k}) \tag{32}$$

The flux of $\boldsymbol{F}'$ and $\boldsymbol{G}'$ can be obtained similarly, following the symmetric rule in the η and ζ directions.

When the control volume method is used, the discretized governing equation (29) can be rewritten in the following integral form:

$$\begin{aligned}\frac{\partial}{\partial t}\int \boldsymbol{Q}'\,\mathrm{d}\xi\,\mathrm{d}\eta\,\mathrm{d}\zeta&+\left(\boldsymbol{E}'_{i+\frac12}-\boldsymbol{E}'_{i-\frac12}\right)+\left(\boldsymbol{F}'_{j+\frac12}-\boldsymbol{F}'_{j-\frac12}\right)\\&+\left(\boldsymbol{G}'_{k+\frac12}-\boldsymbol{G}'_{k-\frac12}\right)=\left(\boldsymbol{R}'_{i+\frac12}-\boldsymbol{R}'_{i-\frac12}\right)\\&+\left(\boldsymbol{S}'_{j+\frac12}-\boldsymbol{S}'_{j-\frac12}\right)+\left(\boldsymbol{T}'_{k+\frac12}-\boldsymbol{T}'_{k-\frac12}\right)\end{aligned} \tag{33}$$

By use of the new CUSP scheme, the interface flux $\boldsymbol{E}'_{1/2}$ is evaluated as follows

For $|U|\le a$,

$$\begin{aligned}\boldsymbol{E}'_{\frac12}=&\frac12\left[(\rho U)_{\frac12}\left(\boldsymbol{q}^c_L+\boldsymbol{q}^c_R\right)-|\rho U|_{\frac12}\left(\boldsymbol{q}^c_R-\boldsymbol{q}^c_L\right)\right]\\&+\begin{pmatrix}0\\ \mathcal{P}^+pl_x\\ \mathcal{P}^+pl_y\\ \mathcal{P}^+pl_z\\ \frac12 p\left(U+a_{\frac12}\right)\end{pmatrix}_L+\begin{pmatrix}0\\ \mathcal{P}^-pl_x\\ \mathcal{P}^-pl_y\\ \mathcal{P}^-pl_z\\ \frac12 p\left(U-a_{\frac12}\right)\end{pmatrix}_R\end{aligned} \tag{34}$$

For $U>a$,

$$\boldsymbol{E}'_{\frac12}=\boldsymbol{E}'_L$$

For $U<-a$,

$$\boldsymbol{E}'_{\frac12}=\boldsymbol{E}'_R$$

where

$$\boldsymbol{q}^c=\begin{pmatrix}1\\ u\\ v\\ w\\ e\end{pmatrix} \tag{35}$$

and $(\rho U)_{1/2}$ and $\mathcal{P}^{\pm}$ are evaluated using Eqs. (13–18) and Eq. (22) with u replaced by U.

Equation (3) is updated to include velocity u, v, and w:

$$p=(\gamma-1)\left[\rho e-\tfrac12\rho(u^2+v^2+w^2)\right] \tag{36}$$

V. Results and Discussion

The new E-CUSP scheme will be compared with several other popularly used upwind schemes to study its performance. According to Godunov,[20] when there are discontinuities in the solutions, monotone behavior of a solution can not be assured for a finite difference method with higher than first-order accuracy. Hence, for an upwind scheme to be used as a Riemann solver, it is essential to examine the performance of the scheme using first-order accuracy. For the following test cases, all of the one-dimensional cases and the two-dimensional flat-plate laminar boundary layer use first order accuracy. The transonic nozzle and inlet-diffuser use third-order accuracy for the inviscid fluxes with MUSCL-type differencing[21] and the minmod limiter.

A. Shock Tubes

For shock-tube problems, interest is focused on 1) the quality (monotonicity and sharpness) of the shock and contact discontinuities and 2) the maximum allowable Courant–Friedrichs–Lewy (CFL) number to be used for the explicit Euler method.

For the explicit Euler time-marching scheme, it is desirable that the CFL number be close to the upper limit of 1.0. For the one-dimensional linear wave equation with CFL = 1 and first-order upwind scheme, the numerical dissipation and dispersion vanish. For nonlinear Euler equations, it is also true that the closer the CFL is to 1.0, the less numerical dissipation there is.

1. *Sod Problem*

Figures 1–5 are the computed temperature distributions using different upwind schemes with first-order accuracy, compared with the analytical result of the Sod problem.[22] Because the computation stops before the waves reach either end of the shock tube, the first-order extrapolation boundary conditions are used at both ends of the shock tube for all of the schemes.

The maximum allowable CFL number for a scheme is defined as the CFL number beyond which the solution will either be oscillatory or unstable. The new E-CUSP scheme (Zha CUSP in Fig. 1) achieves

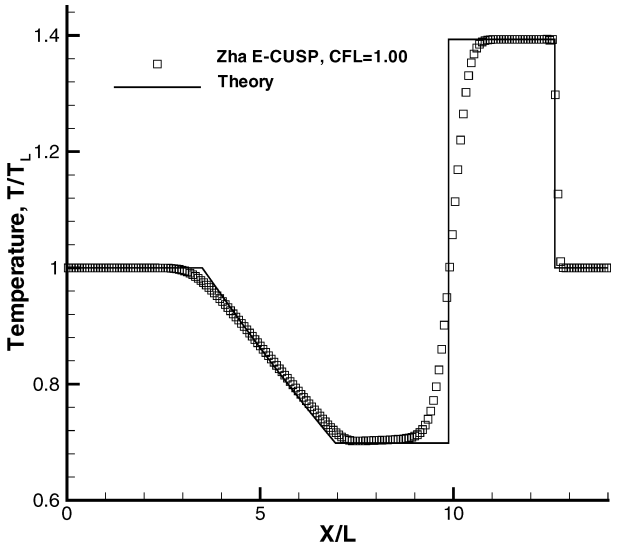

Fig. 1 Temperature distribution of the Sod[22] one-dimensional shock tube computed by Zha E-CUSP scheme.

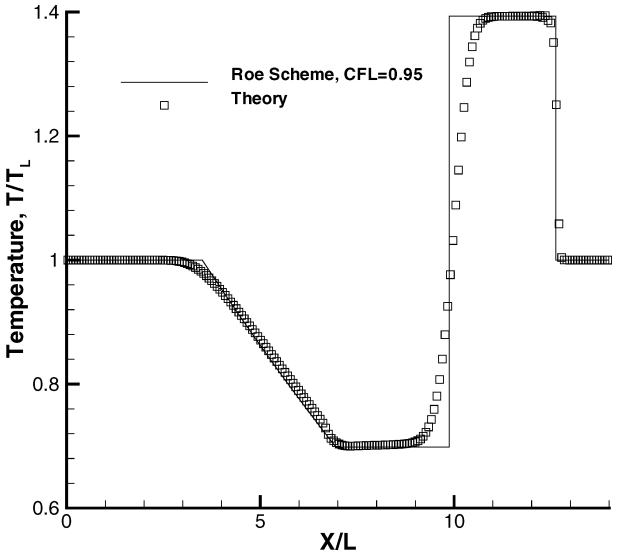

Fig. 2 Temperature distribution of the Sod[22] one-dimensional shock tube computed by the Roe scheme.

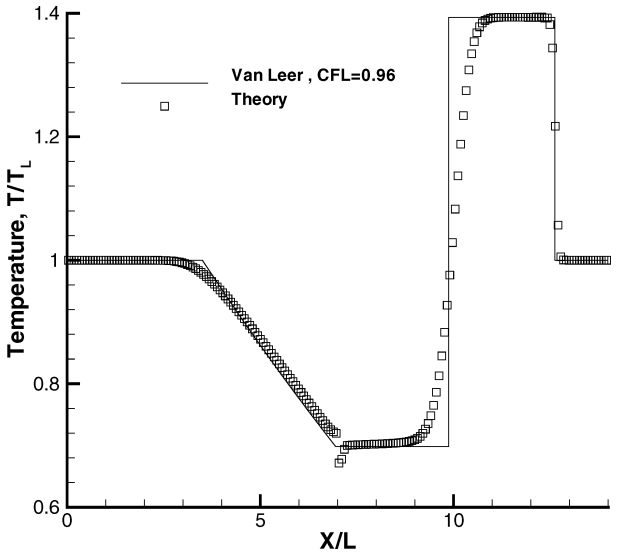

Fig. 3 Temperature distribution of the Sod[22] one-dimensional shock tube computed by the Van Leer scheme.

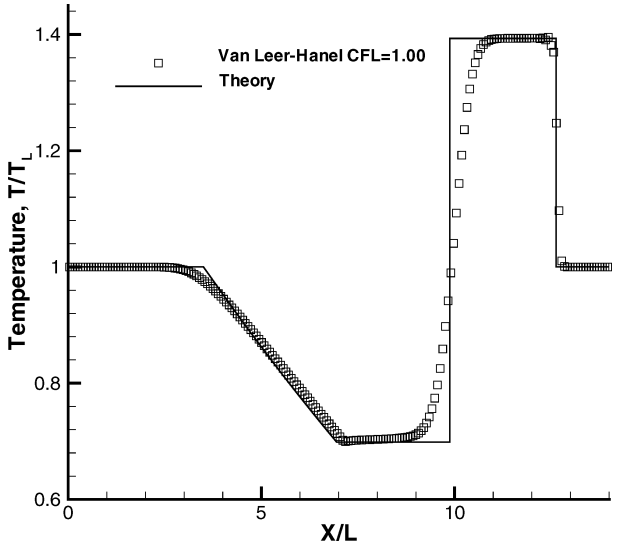

Fig. 4 Temperature distribution of the Sod[22] one-dimensional shock tube computed by Van Leer–Hänel scheme.

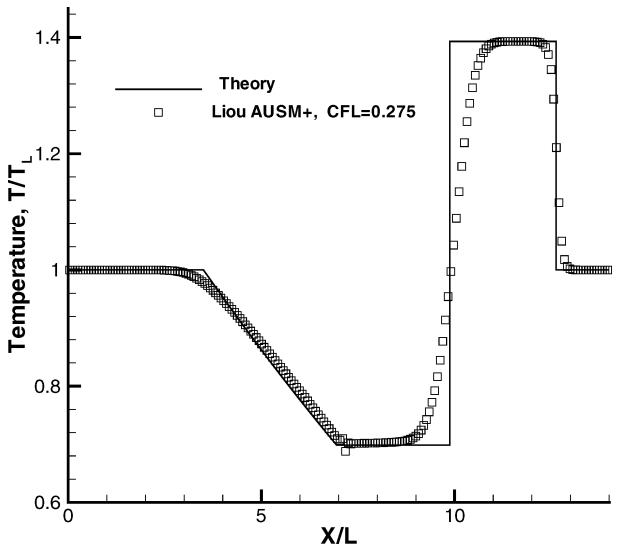

Fig. 5 Temperature distribution of the Sod[22] one-dimensional shock tube computed by the AUSM$^+$ scheme.

maximum CFL of 1.00, and the shock profile is the crispest and remains monotone. The maximum allowable CFLs of the Roe and the Van Leer schemes[18] are 0.95 and 0.96, respectively. The new E-CUSP scheme takes three grid points across the shock wave, whereas the Roe and Van Leer schemes take four grid points (Figs. 1–3). The Van Leer scheme generates a tail at the end of the expansion wave (Fig. 3). Interestingly, the Van Leer–Hänel scheme can reach maximum CFL = 1.0, and the shock profile is also crisper than the original Van Leer scheme with no tail generated at the end of the expansion wave (Fig. 4). All of the schemes smear the contact surface to a similar extent. The expansion wave is captured well by all of the schemes. The AUSM$^+$ scheme has an unexpectedly low maximum allowable CFL of 0.275. The entire shock and contact surface profiles are seriously smeared due to the low maximum CFL number.

Table 1 summarizes the maximum allowable CFL number for each scheme. Overall, for the Sod[22] one-dimensional shock-tube problem, the suggested new scheme performs the best based on shock sharpness, monotonicity, and stability.

2. *Slowly Moving Contact Surface*

This is a shock-tube case used in Ref. 4 to demonstrate the capability of the scheme to capture the contact surface. The initial conditions are $[\rho, u, p]_L = [0.125, 0.112, 1.0]$ and

Table 1 Maximum CFL numbers for Sod[22] one-dimensional shock tube

Scheme	CFL number
New scheme (Zha CUSP)	1.00
Van Leer–Hänel	1.00
Van Leer	0.96
Roe	0.95
Liou AUSM$^+$	0.275

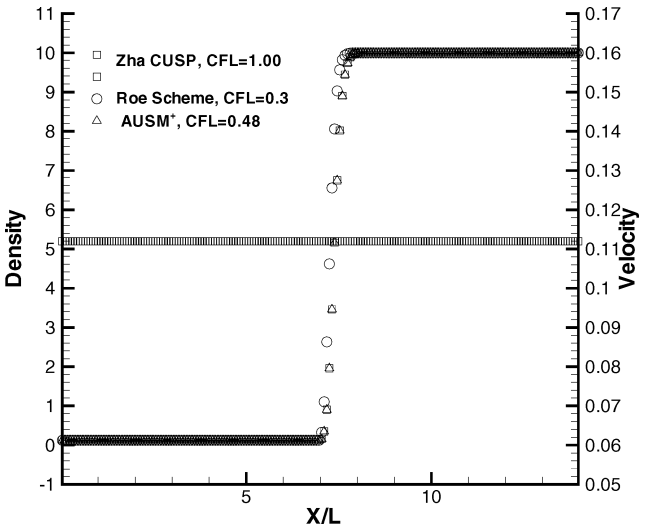

Fig. 6 Computed density and velocity profiles of a slowly moving contact surface.

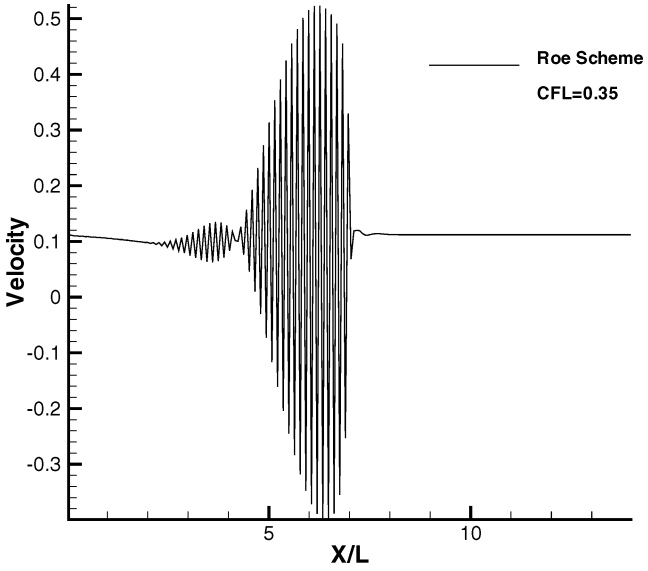

Fig. 7 Computed density profile of a slowly moving contact surface using the Roe scheme.

$[\rho, u, p]_R = [10.0, 0.112, 1.0]$. All of the results are first-order accurate. Figure 6 shows that the new E-CUSP scheme, the Roe scheme, and the AUSM$^+$ scheme can all resolve the contact surface accurately as they are designed. The results of those schemes are at time level 0.01. The velocity is uniformly constant, and the density discontinuity is monotone. The new E-CUSP (Zha CUSP) scheme has far higher CFL number than the other schemes, with the value of 1.00. The Roe scheme has maximum CFL = 0.3, and Liou's AUSM$^+$ has 0.48. Figure. 7 shows that the Roe scheme generates large velocity oscillations when CFL = 0.35, greater than its maximum CFL = 0.3.

Table 2 Maximum CFL numbers of the schemes resolving the contact surface

Scheme	CFL number
New E-CUSP (Zha CUSP)	1.00
Liou AUSM$^+$	0.48
Roe	0.32
Van Leer	Fail
Van Leer–Hänel	Fail

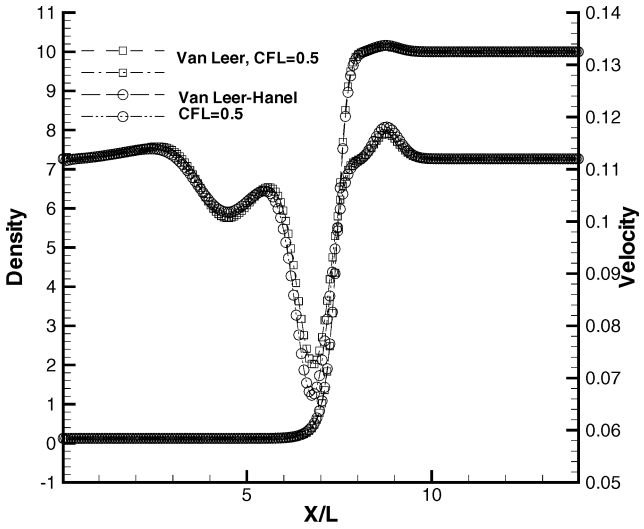

Fig. 8 Computed density and velocity profiles of a slowly moving contact surface.

The schemes of Van Leer and Van Leer–Hänel severely distort the profiles of the contact surfaces, as shown in Fig. 8. The velocity profiles are largely oscillatory. The density jumps are also more smeared.

Table 2 lists the maximum CFL number of each scheme for the slowing moving contact surface. Again, the new scheme outperforms the other schemes by having the highest CFL number and still maintaining the monotonicity.

B. Entropy Condition

This case is used to test whether a scheme violates the entropy condition by allowing the expansion shocks. The test case is a simple quasi-one-dimensional converging–diverging transonic nozzle.[15,16] The correct solution should be a smooth flow from subsonic to supersonic with no shock. However, for an upwind scheme, which does not satisfy the entropy condition, an expansion shock may be produced.

For the subsonic boundary conditions at the entrance, the velocity is extrapolated from the inner domain, and the other variables are determined by the total temperature and total pressure. For supersonic exit boundary conditions, all of the variables are extrapolated from inside of the nozzle. The analytical solution was used as the initial flowfield. The explicit Euler time-marching scheme was used to seek the steady-state solutions. All of the schemes use first-order differencing.

Figure 9 shows the comparison of the analytical and computed Mach number distributions with 201 mesh points using the new scheme and the schemes of Roe, Van Leer, Van Leer–Hänel, and the Liou AUSM$^+$. The analytical solution is smooth throughout the nozzle and reaches the sonic speed at the throat (the minimum area of the nozzle, located at $X/h = 4.22$). It is seen that both the Roe scheme and Van Leer scheme generate a strong expansion shock at the nozzle throat. Both schemes can converge to machine zero (12 order of magnitude) with CFL = 0.95, even with the expansion shock waves.

The Van Leer–Hänel scheme cannot converge, even with CFL = 0.01. The result plotted in Fig. 9 is the one before it diverges.

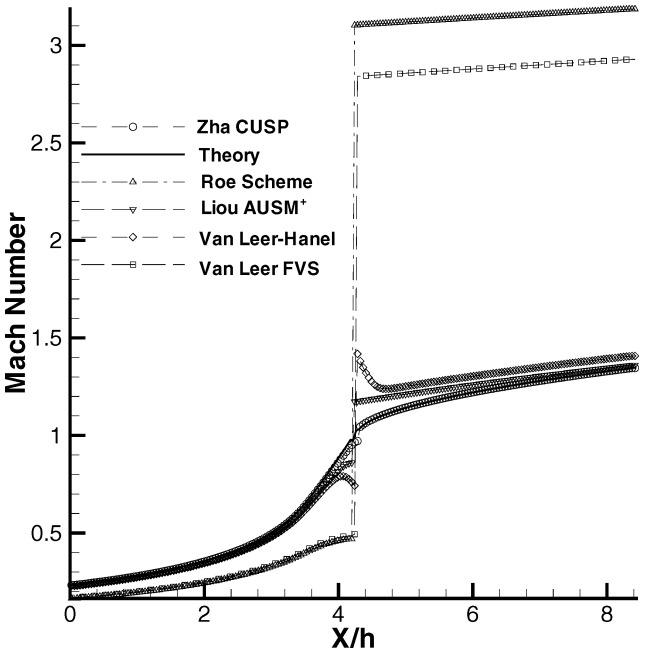

Fig. 9 Computed Mach number distributions for the converging–diverging nozzle.

It shows an expansion shock with the Mach number jumping from 0.74 to 1.42. The AUSM$^+$ also has difficulties converging for this case. With CFL = 0.05, it managed to reduce the residual by four orders of magnitude. The solution of the AUSM$^+$ also shows an expansion shock with the Mach number jumping from 0.86 to 1.17.

The new E-CUSP scheme does not have an expansion shock wave at the sonic point, but is not smooth due to the discontinuity of the first derivative of the pressure at the sonic point. This is shown as a small glitch at the sonic point in Fig. 9. The glitch does not affect the scheme's ability to converge the solution to machine zero with CFL = 0.95.

As indicated in Refs. 15 and 16, the amplitude of the expansion shock decreases when the mesh is refined. When the second-order schemes with the MUSCL differencing are used, all of the expansion shock waves, as well as the glitch of the new scheme at the sonic point, disappear. Because the purpose of this paper is to compare the original Riemann solver schemes, no entropy fix[23] that can remove the expansion shock of Roe schemes was used.

C. Wall Boundary Layer

To examine the numerical dissipation of the new scheme, a laminar supersonic boundary layer on an adiabatic flat plate is calculated using first-order accuracy. The incoming Mach number is 2.0. The Reynolds number based on the length of the flat plate is 4×10^4. The Prandtl number of 1.0 is used to compare the numerical solutions with the analytical solution. The baseline mesh size is 81×61 in the direction along the plate and normal to the plate, respectively.

Figure 10 shows the comparison between the computed velocity profiles and the Blasius solution. The solutions of the new scheme (Zha CUSP), Roe scheme, and AUSM$^+$ scheme agree very well with the analytical solution. The Van Leer scheme significantly thickens the boundary layer. The Van Leer–Hänel scheme does not improve the velocity profile.

Figure 11 shows the comparison between the computed temperature profiles and the Blasius solution. Again, the new scheme (Zha CUSP), Roe scheme, and AUSM$^+$ scheme accurately predict the temperature profiles, and the computed solutions basically go through the analytical solution. Both the Van Leer scheme and the Van Leer–Hänel scheme significantly thicken the thermal boundary layer, similarly to the velocity profiles.

Table 3 shows the wall temperature predicted by all of the schemes using the baseline mesh and refined mesh. The predicted temperature value by the Van Leer scheme has a large error. The Van Leer–Hänel scheme does predict the wall temperature accurately, even though the overall profile is nearly as poor as that predicted by the Van Leer scheme. The new scheme, Roe scheme, and AUSM+ scheme all predict the temperature accurately.

Table 3 Computed nondimensional wall temperature using first-order schemes with baseline mesh and refined mesh

Scheme	T_{wall}, mesh 80×60	T_{wall}, mesh 160×120
Blasius analytical solution	1.8000	1.8000
New E-CUSP (Zha CUSP)	1.8025	1.8018
Roe	1.8002	1.7996
Liou AUSM$^+$	1.8000	1.8000
Van Leer	1.8328	1.8333
Van Leer–Hänel	1.7970	1.7996

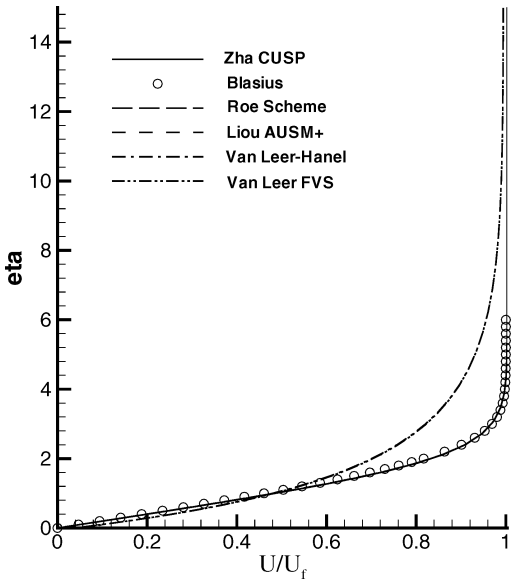

Fig. 10 Computed velocity profiles of the laminar boundary layer using first-order schemes.

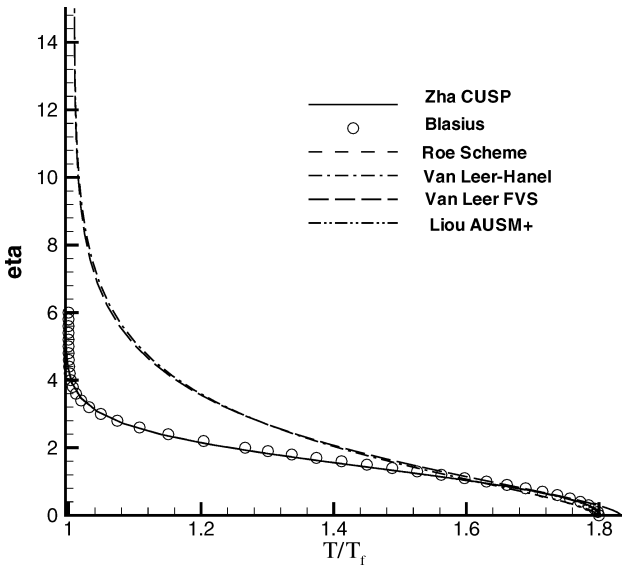

Fig. 11 Computed temperature profiles of the laminar boundary layer using first-order schemes.

All of the mentioned results are converged based on mesh size. The wall temperatures using the refined mesh of 161×121 are also given in Table 3. There is little difference between the results of the baseline mesh and the refined mesh. The refined mesh does not help to reduce the large numerical dissipation of the Van Leer scheme.

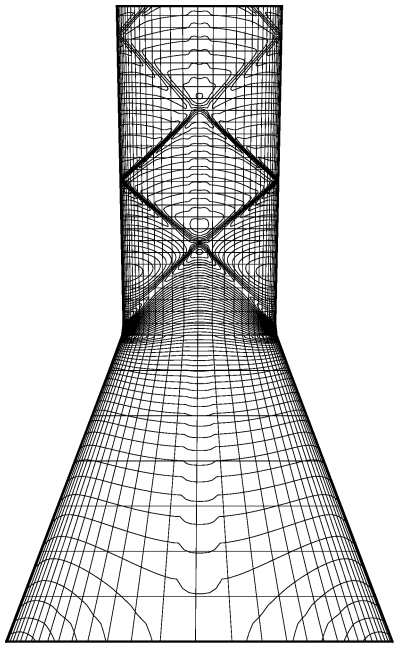

Fig. 12 Computed Mach number contours using the Zha CUSP scheme.

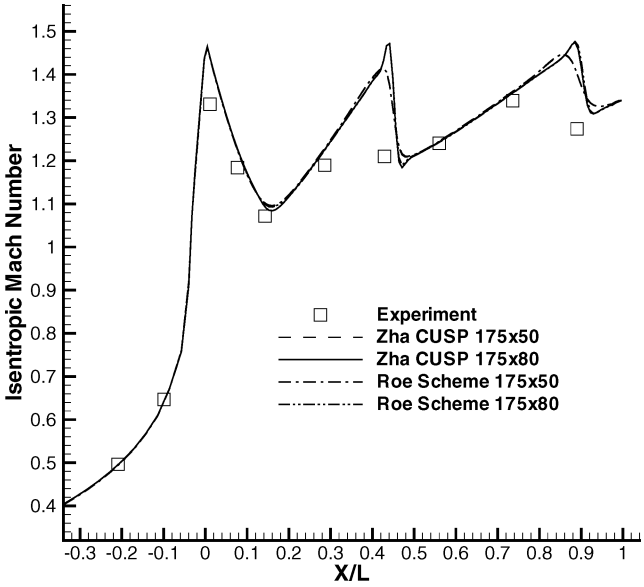

Fig. 13 Adiabatic Mach number distribution computed on the wall surface of the nozzle.

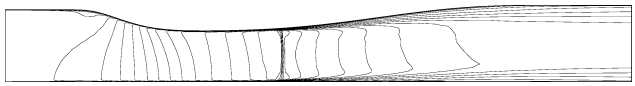

Fig. 14 Computed Mach number contours using the Zha CUSP scheme with $p_{out}/p_t = 0.83$.

When the second-order schemes are used, both the velocity and temperature profiles of the Van Leer and Van Leer–Hänel schemes are improved (not shown).

D. Transonic Converging–Diverging Nozzle

To examine the performance of the new scheme in two-dimensional flow and the capability to capture the shock waves that do not align with the mesh lines, a transonic converging–diverging nozzle is calculated as inviscid flow. The nozzle was designed and tested at NASA and was named nozzle A1.[24] Third-order accuracy of MUSCL-type differencing is used to evaluate the inviscid flux with the minmod limiter. Figure 12 is the computed Mach number contour using the new E-CUSP scheme with the mesh size of 175×80. In the axial direction, there are 140 mesh points distributed downstream of the nozzle throat, where the oblique shock waves are located. The grid is clustered near the wall. For clarity, the coarsened mesh is drawn as the background with the Mach contours to show the relative orientation of the shock waves and the mesh lines. The nozzle is symmetric about the centerline; hence, only the upper half of the nozzle is calculated. The upper boundary uses the slip wall boundary conditions and the lower boundary of the centerline uses the symmetric boundary conditions.

As indicated by the wall surface isentropic Mach number distribution shown in Fig. 13, the flow is subsonic at the inlet with a Mach number of about 0.22, is accelerated to sonic at the throat, and then reaches supersonic with a Mach number of about 1.35 at the exit. Figure 12 shows that, right after the throat, an expansion fan emanates from the wall and accelerates the flow to reach the peak Mach number about 1.5. Because of the sharp throat turning, an oblique shock appears immediately downstream of the expansion fan and turns the flow to the axial direction. The two oblique shocks intersect at the centerline, go through each other, hit the wall on the other side, and then reflect from the wall. This shock patten is repeated to the exit, and the shock strength is weakened with the flow going downstream. Figure 13 shows that the isentropic Mach number distributions predicted by the new CUSP scheme and the Roe scheme agree fairly well with the experiment. The new E-CUSP scheme and the Roe scheme have virtually indistinguishable results.

The mesh refinement study indicates that the mesh resolution in the axial direction does not affect the shock resolution much. The axial mesh size of 280 downstream of the throat yields only slightly better shock resolution than the mesh size of 70. However, the mesh size in the vertical direction dramatically changes the shock resolution. The mesh size of 80 in the vertical direction yields much better resolution than the mesh size of 50. This can be seen from the isentropic Mach number in Fig. 13, which shows that the mesh size of 175×80 generates much sharper profiles than those of the mesh 175×50 for the first and second shock reflections.

For this transonic nozzle with the mesh size 175×80 on an Intel Xeon 1.7 GHz processor, the CPU time per time step per node to calculate the inviscid flux is 2.5871×10^{-6} s for the new scheme, which is about 25% of the CPU time of 1.0284×10^{-5} s used for the Roe scheme. This is a significant CPU time reduction.

E. Transonic Inlet-Diffuser

To examine the performance of the new scheme for shock wave/turbulent boundary-layer interaction, a transonic inlet-diffuser,[25] which has the exit back pressure equal to 0.83 times of the inlet total pressure, is calculated as shown by the Mach number contours in Fig. 14. The Reynolds number based on the throat height is 4.38×10^5. The Baldwin–Lomax[26] algebraic turbulence model is used. Third-order accuracy of MUSCL-type differencing with the minmod limiter is used for the inviscid fluxes, and the second-order central differencing is used for the viscous terms.

A normal shock is located downstream of the throat, as shown in Fig. 14. No flow separation is generated under this backpressure. The baseline mesh size is 100×60. When y_1^+ is held as constant and the mesh is refined in both the horizontal and vertical directions, the results have little variation and are converged based on mesh size. All of the inlet-diffuser results presented are from the mesh size of 100×120. The mesh in the horizontal direction is clustered around the shock location to better resolve the shock profile.

Figure 15 shows the comparison of the upper wall surface pressure between the experiment and the computation. The agreement is very good, except that the computation predicts the shock location a little downstream of the experimental shock location and a shock strength that is a little too strong. It is found that the shock profile is sensitive to y_1^+. The y_1^+ values of $2, 2 \times 10^{-4}, 7 \times 10^{-6}$ are tested. The smaller y_1^+ yields a shock location that is a little closer to that of the experiment. The results shown in Figs. 14 and 15 have a y_1^+ value of 2×10^{-4}. The small y_1^+ effect is believed to be due

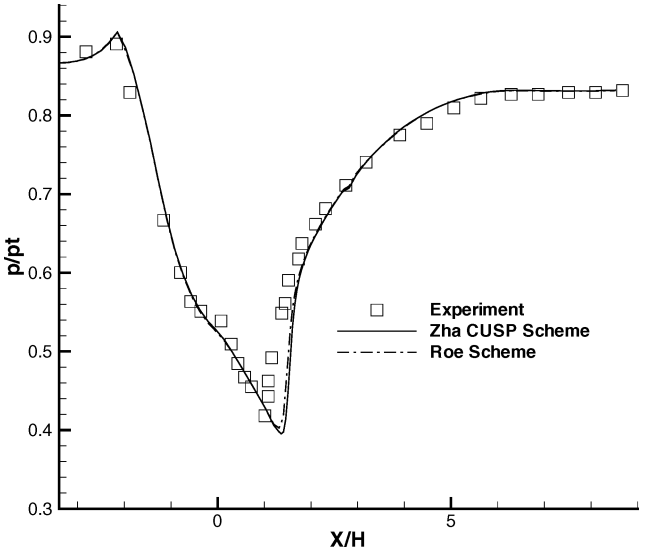

Fig. 15 Static pressure distribution computed on the upper surface of the inlet-diffuser ($p_{out}/p_t = 0.83$).

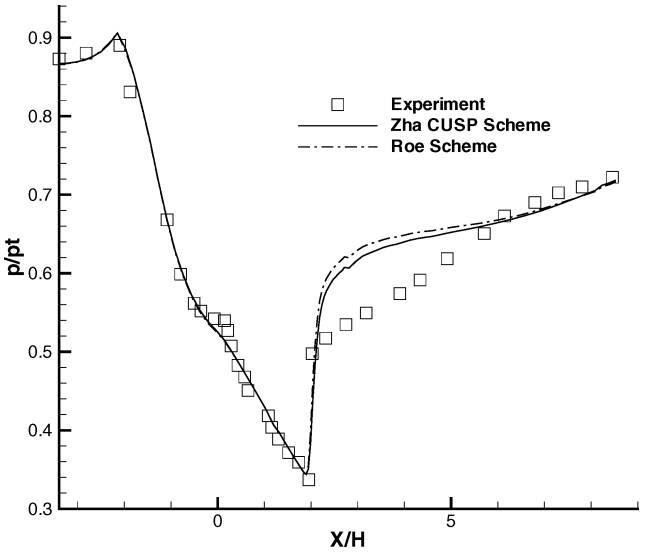

Fig. 16 Static pressure distribution computed on the upper surface of the inlet-diffuser ($p_{out}/p_t = 0.72$).

to the first-order extrapolation of the pressure on the wall surface instead of the requirement of the turbulence modeling. In the region with no shock, the first-order pressure extrapolation on the wall is insensitive to the distance of the first cell to the wall, whereas in the shock region it is sensitive due to the large streamwise gradient. As indicated in Fig. 15, the Roe scheme predicts the shock location slightly closer to the experiment than the new CUSP scheme.

When the backpressure is reduced to 0.72 times the inlet total pressure, the normal shock is stronger, and flow separation is induced. The same mesh as that the previous case is used for this case. Figure 16 is the predicted pressure distribution compared with the experiment. Both the new CUSP scheme and the Roe scheme predict the shock location accurately, but the shock strength predicted is too strong. However, the new scheme has the pressure profile in the separation region downstream of the shock noticeably closer to the experiment than that predicted by the Roe scheme.

Note that the turbulence modeling is a critical factor for the prediction accuracy of the shock wave/turbulent boundary-layer interaction. Hence, the discrepancy between the calculation and experiment shown earlier is only partially attributed to the different discretization schemes.

Figure 17 shows the pressure contours computed using $p_{out}/p_t = 0.72$ with the new scheme, the Roe scheme, and the Liou

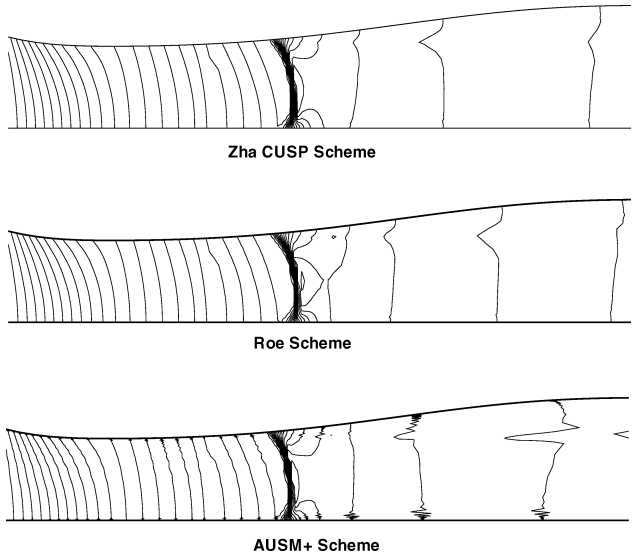

Fig. 17 Comparison of computed pressure contours using the Zha CUSP scheme, the Roe scheme, and the Liou AUSM$^+$ scheme ($p_{out}/p_t = 0.72$).

AUSM$^+$ scheme. A curved λ shock is formed due to the shock wave/turbulent boundary-layer interaction. The shape of the Mach contours of the new scheme (Zha CUSP) and the Roe scheme are very much alike. The contours computed by the AUSM$^+$ scheme have significant oscillations near the wall.

VI. Conclusions

A new efficient upwind scheme based on the CUSP concept is developed. The upwinding of the convective term and the pressure splitting are consistent with their characteristics directions. The numerical dissipation of the new scheme at stagnation is low and is not greater than that of the Roe scheme. Hence, the scheme is able to resolve accurately wall boundary layers and is able to capture crisp shock waves and exact contact discontinuities. The performance of the new scheme is compared with the Roe scheme, AUSM$^+$ scheme, Van Leer scheme, and Van Leer–Hänel scheme.

For the one-dimensional Sod[22] shock-tube problem using the Euler explicit scheme, the new scheme has the crispest shock profile and highest allowable CFL of 1.0. For a slowly moving contact surface, the new scheme is demonstrated to capture the exact contact surface discontinuity with the maximum allowable CFL of 1.0, which is far greater than that of the other schemes. For a quasi-one-dimensional transonic nozzle, all of the other schemes generate expansion shocks at the sonic point. The new scheme does not have the expansion shock, although it has a glitch at the sonic point, which is due to the discontinuity of the first derivative of the pressure splitting at the sonic point.

For a Mach = 2.0 supersonic adiabatic laminar flat-plate boundary layer, the new scheme is able to resolve accurately the boundary-layer velocity and temperature profiles using first-order differencing. The solution is as accurate as that of the Roe scheme and the AUSM$^+$ scheme and, hence, demonstrates the low diffusion of the new scheme.

For a transonic converging–diverging nozzle, oblique shock waves and reflections are crisply captured although the shock waves do not align with the mesh lines. The predicted wall surface isentropic Mach number distribution agrees well with the experiment. For a transonic inlet-diffuser with shock/turbulent boundary-layer interaction, the new scheme and the Roe scheme predict the surface pressure distributions, agreeing well with the experiment for the case of a weak shock. For the strong shock case, both the new scheme and the Roe scheme overpredict the strength of the shock wave. However, the pressure distribution predicted by the new scheme is closer to the experiment. The AUSM$^+$ solution has large pressure oscillations.

In conclusion, the new scheme is proved to be accurate, robust, and efficient for the flow cases tested.

Acknowledgments

This work is partially supported by Air Force Office of Scientific Research Grant F49620-03-1-0253 monitored by William Hilbun.

References

[1]Roe, P., "CFD Algorithms," NASA Spring Workshop on Fluids, April 2003.

[2]Roe, P., "Approximate Riemann Solvers, Parameter Vectors, and Difference Schemes," *Journal of Computational Physics*, Vol. 43, 1981, pp. 357–372.

[3]Liou, M.-S., and Steffen, C. J., "A New Flux Splitting Scheme," *Journal of Computational Physics*, Vol. 107, 1993, pp. 1–23.

[4]Wada, Y., and Liou, M.-S., "An Accurate and Robust Splitting Scheme for Shock and Contact Discontinuities," AIAA Paper 94-0083, Jan. 1994.

[5]Liou, M.-S., "A Sequel to AUSM: AUSM$^+$," *Journal of Computational Physics*, Vol. 129, 1996, pp. 364–382.

[6]Liou, M.-S., "A Sequel to AUSM: AUSM$^+$," *Journal of Computational Physics*, Vol. 129, 1996, pp. 364–382.

[7]Liou, M.-S., "Ten Years in the Making—AUSM-Family," AIAA Paper 2001-2521, June 2001.

[8]Hänel, D., Schwane, R., and Seider, G., "On the Accuracy of Upwind Schemes for the Solution of the Navier–Stokes Eqautions," AIAA Paper 87-1105-CP, 1987.

[9]Edwards, J. R., "A Low-Diffusion Flux-Splitting Scheme for Navier–Stokes Calculations," AIAA Paper 95-1703-CP, June 1995.

[10]Edwards, J. R., "A Low-Diffusion Flux-Splitting Scheme for Navier–Stokes Calculations," *Computer and Fluids*, Vol. 6, 1997, pp. 635–659.

[11]Jameson, A., "Analysis and Design of Numerical Schemes for Gas Dynamics I: Artificial Diffusion, Upwind Biasing, Limiters and Their Effect on Accuracy and Multigrid Convergence in Transonic and Hypersonic Flow," AIAA Paper 93-3359, July 1993.

[12]Jameson, A., "Analysis and Design of Numerical Schemes for Gas Dynamics I: Artificial Diffusion, Upwind Biasing, Limiters and Their Effect on Accuracy and Multigrid Convergence in Transonic and Hypersonic Flow," *Journal of Computational Fluid Dynamics*, Vol. 4, 1995, pp. 171–218.

[13]Jameson, A., "Analysis and Design of Numerical Schemes for Gas Dynamics II: Artificial Diffusion and Discrete Shock Structure," *Journal of Computational Fluid Dynamics*, Vol. 5, 1995, pp. 1–38.

[14]Zha, G.-C., and Bilgen, E., "Numerical Solutions of Euler Equations by Using a New Flux Vector Splitting Scheme," *International Journal for Numerical Methods in Fluids*, Vol. 17, 1993, pp. 115–144.

[15]Zha, G.-C., "Numerical Tests of Upwind Scheme Performance for Entropy Condition," *AIAA Journal*, Vol. 37, 1999, pp. 1005–1007.

[16]Zha, G.-C., "Numerical Tests of Upwind Scheme Performance for Entropy Condition," *AIAA Journal*, Vol. 37, No. 8, 1999, pp. 1005–1007; also AIAA Paper 99-3348, June–July 1999.

[17]Steger, J., and Warming, R., "Flux Vector Splitting of the Inviscid Gasdynamic Equations with Application to Finite-Difference Methods," *Journal of Computational Physics*, Vol. 40, 1981, pp. 263–293.

[18]Van Leer, B., "Flux-Vector Splitting for Euler Equations," *Lecture Notes in Physics*, Vol. 170, 1982, pp. 507–512.

[19]Van Leer, B., Thomas, J., Roe, P. L., and Newsome, R., "A Comparison of Numerical Flux Formulas for the Euler and Navier–Stokes Equations," AIAA Paper 87-1104, 1987.

[20]Godunov, S., "Finite-Difference Method for Numerical Computation of Discontinuous Solutions of the Equations of Fluid Dynamics," *Math Sbornik*, Vol. 47, 1959, pp. 271–306 (in Russian) (translated by U.S. Joint Publication Research Service, JPRS 7226, 1969).

[21]Van Leer, B., "Towards the Ultimate Conservative Difference Scheme, III," *Journal of Computational Physics*, Vol. 23, 1977, pp. 263–275.

[22]Sod, G., "A Survey of Several Finite Difference Methods for Systems of Nonlinear Hyperbolic Conversation Laws," *Journal of Computational Physics*, Vol. 27, 1978, pp. 1–31.

[23]Harten, A., Lax, P. D., and Van Leer, B., "On Upstream Differencing and Godunov-Type Scheme for Hyperbolic Conservation Laws," *SIAM Review*, Vol. 25, No. 1, 1983, pp. 35–61.

[24]Mason, M. L., and Putnam, L. E., "The Effect of Throat Contouring on Two-Dimensional Converging–Diverging Nozzles at Static Conditions," NASA TP 1704, 1980.

[25]Bogar, T., Sajben, M., and Kroutil, J., "Characteristic Frequency and Length Scales in Transonic Diffuser Flow Oscillations." AIAA Paper 81-1291, June 1981.

[26]Baldwin, B., and Lomax, H., "Thin Layer Approximation and Algebraic Model for Separated Turbulent Flows," AIAA Paper 78-257, 1978.

P. Givi
Associate Editor